Performances of site specific parameterizations of longwave radiation

Giuseppe Formetta[1], Marialaura Bancheri[2], Olaf David [3] and Riccardo Rigon [2]

[1]Centre for Ecology & Hydrology, Crowmarsh Gifford, Wallingford, UK

[2]Dipartimento di Ingegneria Civile Ambientale e Meccanica, Universita' degli Studi di Trento, Italy

[3]Dept. of Civil and Environmental Engineering, Colorado State University, Fort Collins, CO, USA

September 20, 2016

Abstract

In this work ten algorithms for estimating downwelling longwave atmospheric radiation ($L_{\downarrow}$) and one for upwelling longwave radiation ($L_{\uparrow}$) are integrated into the JGrass-NewAge modeling system. The algorithms are tested against energy flux measurements available for 24 sites in North America to assess their reliability. These new JGrass-NewAge model components are used i) to evaluate the performances of simplified models (SMs) of $L_{\downarrow}$, as presented in literature formulations, and ii) to determine by automatic calibration the site-specific parameter sets for $L_{\downarrow}$ in SMs. For locations where calibration is not possible because of a lack of measured data, we perform a multiple regression using on-site variables, i.e. mean annual air temperature, relative humidity, precipitation, and altitude. The regressions are verified through a leave-one-out cross validation, which also gathers information about the possible errors of estimation. Most of the SMs, when executed with parameters derived from the multiple regressions, give enhanced performances compared to the corresponding literature formulation. A sensitivity analysis is carried out for each SM to understand how small variations of a given parameter influence SM performance. Regarding the $L_{\downarrow}$ simulations, the Brunt (1932) and Idso (1981) SMs, in their literature formulations, provide the best performances in many of the sites. The site-specific parameter calibration improves SM performances compared to their literature formulations. Specifically, the root mean square error (RMSE) is almost halved and the Kling Gupta efficiency is improved at all sites.

The $L_{\uparrow}$ SM is tested by using three different temperatures (surface soil temperature, air temperature at 2 m elevation, and soil temperature at 4 cm depth) and model performances are then assessed. Results show that the best performances are achieved using the surface soil temperature and the air temperature.

1 Introduction

Longwave radiation (4-100 μm) is an important component of the radiation balance on earth and it affects many phenomena, such as evapotranspiration, snow melt (Plüss and Ohmura, 1997), glacier evolution (MacDonell et al., 2013), vegetation dynamics (Rotenberg et al., 1998), plant respiration, and primary productivity (Leigh Jr, 1999). Longwave radiation is usually measured with pyrgeometers, but these are not normally available in basic meteorological stations, even though an increasing number of projects has been developed to fill the gap (Augustine et al., 2000), as seen in Augustine et al. (2005) and Baldocchi et al. (2001). The use of satellite products to estimate longwave solar radiation is increasing (GEWEX, Global Energy and Water cycle Experiment, ISCCP the International Satellite Cloud Climatology Project) but they have too coarse a spatial resolution for many hydrological uses. Therefore, models have been developed to solve energy transfer equations and compute radiation at the surface (e.g. Key and Schweiger (1998), Kneizys et al. (1988)). These physically based and fully distributed models provide accurate estimates of the radiation components. However, they require input data and model parameters that are not easily available. To overcome this issue, simplified models (SM), which are based on empirical or physical conceptualizations, have been developed to relate longwave radiation to atmospheric proxy data such as air temperature, water vapor deficit, and shortwave radiation. They are widely used and provide clear sky (e.g. Ångström (1915); Brunt (1932); Idso and Jackson (1969)) and all-sky estimations of downwelling ($L_{\downarrow}$) and upwelling ($L_{\uparrow}$) longwave radioation(e.g. Brutsaert (1975); Iziomon et al. (2003a)).

SM performances have been assessed in many studies by comparing measured and modeled $L_{\downarrow}$ at hourly and daily time-steps (e.g. Sugita and Brutsaert (1993b); Iziomon et al. (2003b); Juszak and Pellicciotti (2013); MacDonell et al. (2013); Schmucki et al. (2014)). Hatfield et al. (1983) was among the first to present a comparison of the most used SMs in an evaluation of their accuracy. They tested seven clear-sky algorithms using atmospheric data from different stations in the United States. In order to validate the SMs under different climatic conditions, they performed linear regression analyses on the relationship between simulated and measured $L_{\downarrow}$ for each algorithm. The results of the study show that the best models were Brunt (1932), Brutsaert (1975) and Idso (1981). Flerchinger et al. (2009) made a similar comparison using more formulations (13) and a wider data-set from North America and China, considering all possible sky conditions. Finally, Carmona et al. (2014) evaluated the performance of six SMs, with both literature and site-specific formulations, under clear-sky conditions for the sub-humid Pampean region of Argentina.

However, none of the above studies have: i) developed a method to systematically compute the site-specific model parameters for location where measurements are available, and ii) provided their estimate for any location based on basic site characteristics. Moreover, differently from other studies, all the tools used in this paper are open-source, well documented, and ready for practical use by other researchers and practitioners.

This paper introduces the LongWave Radiation Balance package (LWRB) of the JGrass-NewAGE modelling system Formetta et al. (2014a). LWRB implements 10 formulations for $L_{\downarrow}$ and one for $L_{\uparrow}$ longwave radiation. The package was systematically tested against measured $L_{\downarrow}$ and $L_{\uparrow}$ longwave radiation data from 24 stations

across the USA, chosen from the 65 stations of the AmeriFlux Network. Unlike all previous works, the LWRB component follows the specifications of the Object Modeling System (OMS) framework (David et al., 2013). Therefore, it can use all of the JGrass-NewAge tools for the automatic calibration algorithms, data management and GIS visualization, and it can be seamlessly integrated into various modeling solutions for the estimation of water budget fluxes (Formetta et al., 2014a).

2 Methodology

The SMs for $L_{\uparrow}$ [Wm^{-2}] and $L_{\downarrow}$ [Wm^{-2}] longwave radiation are based on the Stefan-Boltzmann equation:

$$L_{\downarrow} = \epsilon_{all-sky} \cdot \sigma \cdot T_a^4 \tag{1}$$

$$L_{\uparrow} = \epsilon_s \cdot \sigma \cdot T_s^4 \tag{2}$$

where $\sigma = 5.670 \cdot 10^{-8}$ [W m^{-2} K^{-4}] is the Stefan-Boltzmann constant, T_a [K] is the air temperature, $\epsilon_{all-sky}$ [-] is the effective atmospheric emissivity, ϵ_s [-] is the soil emissivity and T_s [K] is the surface soil temperature. To account for the increase of $L_{\downarrow}$ in cloudy conditions, $\epsilon_{all-sky}$ [-] is formulated according to eq. (3):

$$\epsilon_{all-sky} = \epsilon_{clear} \cdot (1 + a \cdot c^b) \tag{3}$$

where c [-] is the cloud cover fraction and a [-] and b [-] are two calibration coefficients. Site specific values of a and b are presented in Brutsaert (1975), (a=0.22 and b=1), Iziomon et al. (2003a) (a ranges between 0.25 and 0.4 and b=2) and Keding (1989) (a=0.183 and b=2.18). In our modeling system a and b are calibrated to fit measurement data under all-sky conditions. The cloud cover fraction, c, can be estimated from solar radiation measurements (Crawford and Duchon, 1999), from visual observations (Alados-Arboledas et al., 1995, Niemelä et al., 2001), and from satellite data (Sugita and Brutsaert, 1993a) or it can be modeled as well. In this study we use the formulation presented in Campbell (1985) and Flerchinger (2000), where c is related to the clearness index s [-], i.e. the ratio between the measured incoming solar radiation, I_m [Wm^{-2}], and the theoretical solar radiation computed at the top of the atmosphere, I_{top} [Wm^{-2}], according the following relationship: $c = 1 - s$ (Crawford and Duchon, 1999). This type of formulation needs a shortwave radiation balance model to estimate I_{top} and meteorological stations to measure I_m; also, it cannot estimate c at night. In our application, the fact that the SMs are fully integrated into the JGrass-NewAge system allows us to use the shortwave radiation balance model (Formetta et al., 2013) to compute I_{top}. Night-time values of c are computed with a linear interpolation between its values at the last hour of daylight and the first hour of daylight on consecutive days. The computation of the first and last hour of the day is based on the model proposed in Formetta et al., 2013 that follow the approach proposed in Corripio (2002), equations 4.23-4.25. The sunrise occurs at $t = 12 \cdot (1 - \omega/\pi)$ and the sunset will be at $t = 12 \cdot (1 + \omega/\pi)$ where ω is the hour angle. Those equations are based on the

assumption that sunrise and sunset occur at the time when the z coordinate of the sun vector equals zero.

The formulation presented in equation 3 was proposed by Bolz (1949) applied in other studies (Carmona et al. (2014), Maykut and Church (1973), Jacobs (1978), Niemelä et al. (2001)). Evaluating the effectiveness of different formulations respect to equation 3 is still an open question which is not object of the current paper. It has been investigated in several studies (i.e. Flerchinger et al. (2009), Juszak and Pellicciotti (2013), and citation therein) and some of them recommended the one proposed by Unsworth and Monteith (1975).

Ten SMs from literature have been implemented for the computation of ϵ_{clear}. Table 1 specifies assigned component number, component name, defining equation, and reference to the paper from which it is derived. X, Y and Z are the parameters provided in literature for each model, listed in table 2.

ID	Name	Formulation	Reference
1	Angstrom	$\epsilon_{clear} = X - Y \cdot 10^{Ze}$	Angstrom (1918)
2	Brunt's	$\epsilon_{clear} = X + Y \cdot e^{0.5}$	Brunt's (1932)
3	Swinbank	$\epsilon_{clear} = (X \cdot 10^{-13} \cdot T_a^6)/(\sigma \cdot T_a^4)$	Swinbank (1963)
4	Idso and Jackson	$\epsilon_{clear} = 1 - X \cdot exp(-Y \cdot 10^{-4} \cdot (273 - T_a)^2)$	Idso and Jackson (1969)
5	Brutsaert	$\epsilon_{clear} = X \cdot (e/T_a)^{1/Z}$	Brutsaert (1975)
6	Idso	$\epsilon_{clear} = X + Y \cdot 10^{-4} \cdot e \cdot exp(1500/T_a)$	Idso (1981)
7	Monteith and Unsworth	$\epsilon_{clear} = X + Y \cdot \sigma \cdot T_a^4$	Monteith and Unsworth (1990)
8	Konzelmann	$\epsilon_{clear} = X + Y \cdot (e/T_a)^{1/8}$	Konzelmann et al (1994)
9	Prata	$\epsilon_{clear} = [1 - (X + w) \cdot exp(-(Y + Z \cdot w)^{1/2})]$	Prata (1996)
10	Dilley and O'Brien	$\epsilon_{clear} = (X + Y \cdot (T_a/273.16)^6 + Z \cdot (w/25)^{1/2})/(\sigma \cdot T_a^4)$	Dilley and O'Brien (1998)

Table 1: Clear sky emissivity formulations: T_a is the air temperatue [K], w [kg/m^2] is precipitable water = 4650 [e_0/T_a] and e [kPa] is screen-level water-vapour pressure. The Angstrom and Brunt model was presented as cited by Niemelä et al. (2001). Konzelmann uses water vapour pressure in [Pa] not [kPa].

The models presented in table 1 were proposed with coefficient values (X, Y, Z) strictly related to the location in which the authors applied the model and where measurements of $L_\downarrow$ radiation were collected. Coefficients reflect climatic, atmospheric and hydrological conditions of the sites, and are reported in Table 2.

ID	Name	X	Y	Z
1	Angstrom	0.83	0.18	−0.07
2	Brunt	0.52	0.21	[−]
3	Swinbank	5.31	[−]	[−]
4	Idso and Jackson	0.26	−7.77	[−]
5	Brutsaert	1.72	7	[−]
6	Idso	0.70	5.95	[−]
7	Monteith and Unsworth	−119.00	1.06	[−]
8	Konzelmann et al	0.23	0.48	[−]
9	Prata	1.00	1.20	3.00
10	Dilley and O'brien	59.38	113.70	96.96

Table 2: Model parameter values as presented in their literature formulation.

The formulation of the $L_\uparrow$ requires the soil emissivity, which usually is a property of the nature of a surface, and the surface soil temperature. Table 3 shows the literature values (Brutsaert, 2005) of the soil emissivity for different surface types: ϵ_s varies from a minimum of 0.95 for bare soils to a maximum of 0.99 for fresh snow.

It is well known that surface soil temperature measurements are only available at a few measurement sites. Under the hypothesis that difference between soil and air temperatures is not too big, it is possible to simulate $L_\uparrow$ using the air temperature (Park et al., 2008). In our approach three different types of temperature were

Nature of surface	Emissivity
Bare soil (mineral)	$0.95 - 0.97$
Bare soil (organic)	$0.97 - 0.98$
Grassy vegetation	$0.97 - 0.98$
Tree vegetation	$0.96 - 0.97$
Snow (old)	0.97
Snow (fresh)	0.99

Table 3: Soil emissivity for surface types (Brutsaert, 2005).

used to simulate $L_{\uparrow}$, specifically: surface soil temperature, air temperature at 2 m height, and soil temperature at 4 cm depth.

The LWRB package (see flowchart in figure1) is part of the JGrass-NewAge system and was preliminary tested in Formetta et al. (2014b). Model inputs depend on the specific SM being implemented and the purpose of the run being performed (calibration, verification, simulation). The inputs are meteorological observations such as air temperature, relative humidity, incoming solar radiation, and sky clearness index. The LWRB is also fed by other JGrass-NewAGE components, such as the shortwave radiation balance (SWRB) (Formetta et al., 2013). To test model performances (i.e. verification), the LWRB can be connected to the system's Verification component; to execute the parameter calibration algorithm (Formetta et al., 2014a), it can be connected to the LUCA (Let Us CAlibrate) component. In turn, all these components can and/or need to be connected to other ones, as the problem under examination may require. Model outputs are $L_{\downarrow}$ and $L_{\uparrow}$. These can be provided in single points of specified coordinates or over a whole geographic area, represented as a raster map. For the latter case a digital elevation model (DEM) of the study area is necessary in input.

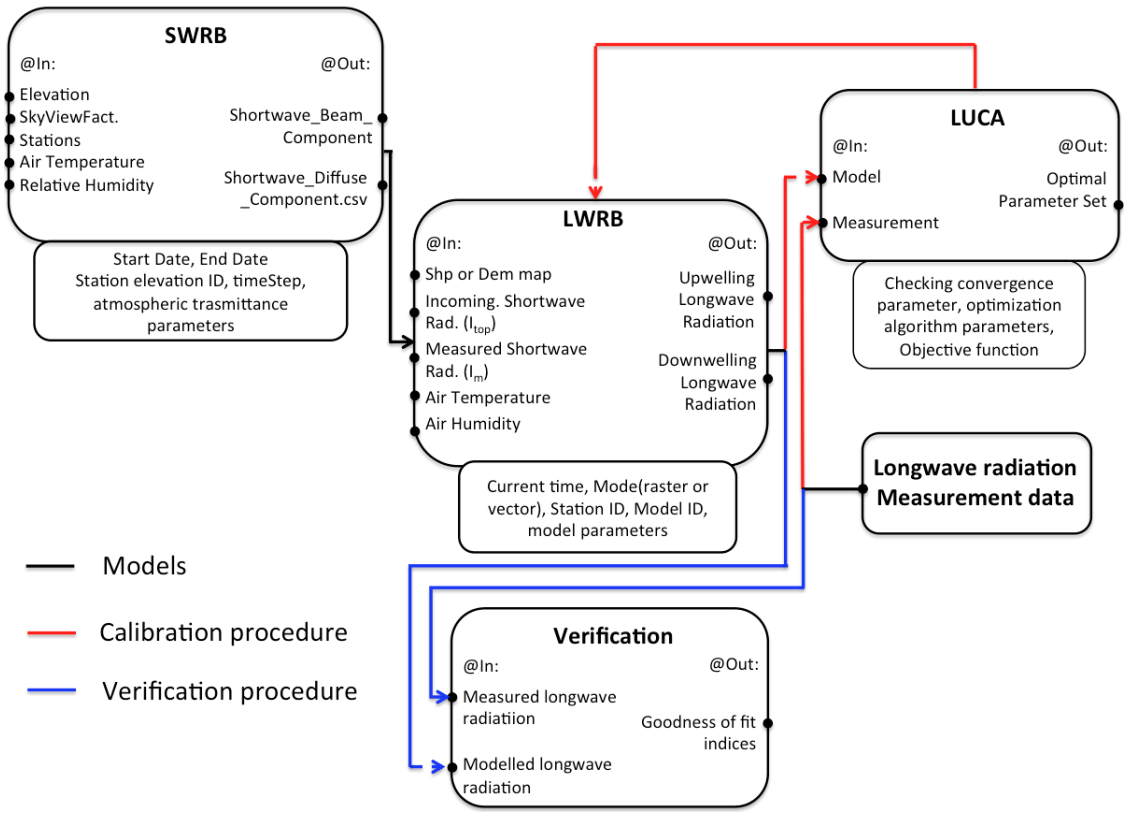

Figure 1: The LWRB component of JGrass-NewAge and the flowchart to model longwave radiation.

The subsection 2.1 and 2.2 respectively present the calibration and the verification procedure. Moreover a model sensitivity analysis procedure is presented in subsection 2.3 and a multi-regression model to relate optimal parameter set and easy available meteorological data is proposed in subsection 2.4.

2.1 Calibration of $L_{\downarrow}$ longwave radiation models

Model calibration estimates the site-specific parameters of $L_{\downarrow}$ models by tweaking them with a specific algorithm in order to best fit measured data. To this end, we use the LUCA calibration algorithm proposed in Hay et al. (2006), which is a part of the OMS core and is able to optimize parameters of any OMS component. LUCA is a multiple-objective, stepwise, and automated procedure. As with any automatic calibration algorithm, it is based on two elements: a global search algorithm; and the objective function(s) to evaluate model performance. In this case, the global search algorithm is the Shuffled Complex Evolution, which has been widely used and described in literature (e.g., Duan et al., 1993). As the objective function we use the Kling-Gupta Efficiency (KGE), which is described below, but LUCA could use other objective functions just as well.

The calibration procedure for $L_{\downarrow}$ follows these steps:

- The theoretical solar radiation at the top of the atmosphere (I_{top}) is computed using the SWRB (see Figure 1);
- The clearness index, c, is calculated as the ratio between the measured incoming solar radiation (I_m) and I_{top};
- Clear-sky and cloud-cover hours are detected by a threshold on the clearness index (equal to 0.6), providing two subsets of measured $L_{\downarrow}$, which are $L_{\downarrow_{clear}}$ and $L_{\downarrow_{cloud}}$. On one side, a threshold of 0.6 to define the clear-sky conditions helps in the sense that allow to define time-series of measured clear-sky $L_{\downarrow}$ with comparable length in all the stations, and this is useful for a reliable calibration process. On the other side, it introduces a small error in computing the emissivity in all-sky condition using equation 3 which could be compensated by the optimization of the parameters a and b;
- The parameters X, Y, and Z for the models in table 1 are optimised using the subset $L_{\downarrow_{clear}}$ and setting a=0 in eq. 3;
- The parameters a and b for eq. 3 are optimized using the subset $L_{\downarrow_{cloud}}$ and using the X, Y, and Z values computed in the previous step.

The calibration procedure provides the optimal set of parameters at a given location for each of the ten models.

As well as parameter calibration, we carry out a model parameter sensitivity analysis and we provide a linear regression model relating a set of site-specific optimal parameters with mean air temperature, relative humidity, precipitation, and altitude.

2.2 Verification of $L_\downarrow$ and $L_\uparrow$ longwave radiation models

As presented in previous applications (e.g. Hatfield et al. (1983), Flerchinger et al. (2009)), we use the SMs with the original coefficients from literature (i.e. the parameters of table 2) and compare the performances of the models against available measurements of $L_\downarrow$ and $L_\uparrow$ for each site. The goodness of fit is evaluated by using two goodness-of-fit estimators: the Kling-Gupta Efficiency (KGE) presented in Gupta et al. (2009); and the root mean square error (RMSE).

The KGE (eq. 4) is able to incorporate into one objective function three different statistical measures of the relation between measured (M) and simulated (S) data: (i) the correlation coefficient, r ; (ii) the variability error, $a = \sigma_S/\sigma_M$; and (iii) the bias error, b=μ_S/μ_M. In these definitions μ_S and μ_M are the mean values, while σ_S and σ_M are the standard deviations, of measured and simulated time series.

$$KGE = 1 - \sqrt{(r-1)^2 + (a-1)^2 + (b-1)^2} \tag{4}$$

The RMSE, on the other hand, is presented in eq. 5:

$$RMSE = \sqrt{\frac{1}{N}\sum_{i=1}^{N}(M_i - S_i)^2} \tag{5}$$

where M and S represents the measured and simulated time-series respectively and N is their length.

2.3 Sensitivity analysis of $L_\downarrow$ models

For each $L_\downarrow$ model we carry out a model parameters sensitivity analysis to investigate the effects and significance of parameters on performance for different model structures (i.e. models with one, two, and three parameters). The analyses are structured according to the following steps:

- we start with the optimal parameter set, computed by the optimization process for the selected model;
- all parameters are kept constant and equal to the optimal parameter set, except for the parameter under analysis;
- 1000 random values of the analyzed parameter are picked from a uniform distribution centered on the optimal value with width equal to ± 30% of the optimal value; in this way 1000 model parameter sets were defined and 1000 model runs were performed;
- 1000 values of KGE are computed by comparing the model outputs with measured time series.

The procedure was repeated for each parameter of each model and for each station of the analyzed dataset.

2.4 Regression model for parameters of $L_\downarrow$ models

The calibration procedure previously presented to estimate the site specific parameters for $L_\downarrow$ models requires measured downwelling longwave data. Because these measurements are rarely available, we implement a

straightforward multivariate linear regression (Chambers et al., 1992; Wilkinson and Rogers, 1973) to relate the site-specific parameters X, Y and Z to a set of easily available site specific climatic variables, used as regressors r_i. To perform the regression we use the open-source R software (https://cran.r-project.org) and to select the best regressors we use algorithms known as "best subsets regression", which are available in all common statistical software packages. The regressors we have selected are: mean annual air temperature, relative humidity, precipitation, and altitude. The models that we use for the three parameters are presented in equations (6), (7), and (8):

$$X = i_X + \sum_{k=1}^{N} \alpha_k \cdot r_k + \epsilon_X \tag{6}$$

$$Y = i_Y + \sum_{k=1}^{N} \beta_k \cdot r_k + \epsilon_Y \tag{7}$$

$$Z = i_Z + \sum_{k=1}^{N} \gamma_k \cdot r_k + \epsilon_Z \tag{8}$$

where N=4 is the number of regressors (annual mean air temperature, relative humidity, precipitation, and altitude); r_k with k=1,.., 4 are the regressors; i_X, i_Y, and i_Z are the intercepts; α_k, β_k, and γ_k are the coefficients; and ϵ_X, ϵ_Y, and ϵ_Z are the normally distributed errors. Once the regression parameters are determined, the end-user can estimate site specific X, Y and Z parameter values for any location by simply substituting the values of the regressors in the model formulations.

3 The study area: the AmeriFlux Network

To test and calibrate the LWRB SMs we use 24 meteorological stations of the AmeriFlux Network (http://ameriflux.ornl.gov). AmeriFlux is a network of sites that measure water, energy, and CO2 ecosystem fluxes in North and South America. The dataset is well-known and used in several applications such as Xiao et al. (2010), Barr et al. (2012), and Kelliher et al. (2004). Data used in this study are the Level 2, 30-minute average data. Complete descriptions and downloads are available at the Web interface located at http://public.ornl.gov/ameriflux/.

We have chosen 24 sites that are representative of most of the USA and span a wide climatic range: going from the arid climate of Arizona, where the average air temperature is 16 °C and the annual precipitation is 350 mm, to the equatorial climate of Florida, where the average air temperature is 24 °C and the annual precipitation is 950 mm. Some general and climatic characteristics for each site are summarized in table 4, while figure 2 shows their locations. The 30-minute average data have been cumulated to obtain continuous time series of averaged, hourly data for longwave radiation, air and soil temperature, relative humidity, precipitation, and soil water content.

SiteID	State	Latitude	Longitude	Elevation (m)	Climate	T (^{o}C)	Data period
1	AZ	31.908	−110.840	991	semiarid	19	2008 – 2013
2	AZ	31.591	−110.509	1469	temperate,arid	16	2002 – 2011
3	AZ	31.744	−110.052	1372	temperate,semi-arid	17	2007 – 2013
4	AZ	31.737	−109.942	1531	temperate,semi-arid	17	2004 – 2013
5	AZ	31.821	−110.866	116	subtropical	19	2004 – 2014
6	AZ	35.445	−111.772	2270	warm temperate	9	2005 – 2010
7	AZ	35.143	−111.727	2160	warm temperate	9	2005 – 2010
8	AZ	35.089	−111.762	2180	warm temperate	8	2005 – 2010
9	CA	37.677	−121.530	323	mild	16	2010 – 2012
10	CA	38.407	−120.951	129	mediterranean	15	2000 – 2012
11	FL	25.365	−81.078	0	equatorial savannah	24	2004 – 2011
12	ME	45.207	−68.725	61	temperate continental	5	1996 – 2008
13	ME	45.204	−68.740	60	temperate continental	6	1996 – 2009
14	MN	44.995	−93.186	301	continental	6	2005 – 2009
15	MN	44.714	−93.090	260	snowy, humid summer	8	2003 – 2012
16	MO	38.744	−92.200	219	temperate continental	13	2004 – 2013
17	MT	48.308	−105.102	634	continental	5	2000 – 2008
18	NJ	39.914	−74.596	30	temperate	12	2005 – 2012
19	OK	36.427	−99.420	611	cool temperate	15	2009 – 2012
20	TN	35.931	−84.332	286	temperate continental	15	2005 – 2011
21	TN	35.959	−84.287	343	temperate	14	1994 – 2007
22	TX	29.940	−97.990	232	warm temperate	20	2004 – 2012
23	WA	45.821	−121.952	371	strongly seasonal	9	1998 – 2013
24	WV	39.063	−79.421	994	temperate	7	2004 – 2010

Table 4: Some general and climatic characteristics of the sites used for calibration: elevation is the site elevation above sea level, T is the annual average temperature, and data period refers to the period of available measurements.

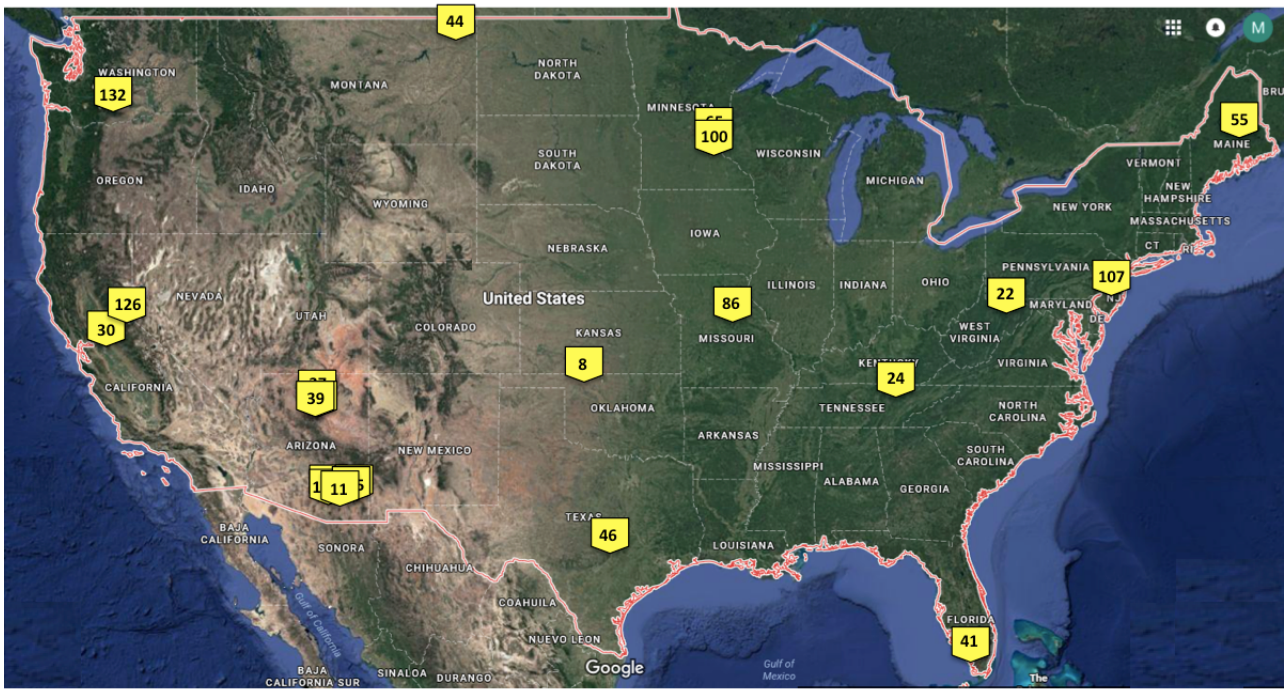

Figure 2: Test site locations in the United State of America.

4 Results

4.1 Verification of $L_\downarrow$ models with literature parameters

When implementing the ten $L_\downarrow$ SMs using the literature parameters, in many cases, they show a strong bias in reproducing measured data. A selection of representative cases is presented in Figure 3, which shows scatterplots

for four SMs in relation to one measurement station. The black points represent the hourly estimates of $L_{\downarrow}$ provided by literature formulations, while the solid red line represents the line of optimal predictions. Model 1 (Ångström (1915)) shows a tendency to lie below the 1:1 line, indicating a negative bias (percent bias of -9.8) and, therefore, an underestimation of $L_{\downarrow}$. In contrast, model 9 (Prata (1996)) shows an overestimation of $L_{\downarrow}$ with a percent bias value of 26.3.

Figure 4 presents the KGE (first column) and RMSE (second column) obtained for each model under clear-sky conditions, grouped by classes of latitude and longitude. Model 8 (Konzelmann et al. (1994)) does not perform very well for many of the stations likely because the model parameters were estimated for the Greenland where the ice plays a fundamental role on the energy balance. Its KGE values range between 0.16 and 0.41, while its RMSE values are higher than 100 W/m^2, with a maximum of 200 W/m^2. Model 6 (Idso (1981)) and model 2 (Brunt (1932)) provide the best results, independently of the latitude and longitude ranges where they are applied. Their KGE values are between 0.75 and 0.94, while the RMSE has a maximum value of 39 W/m^2.

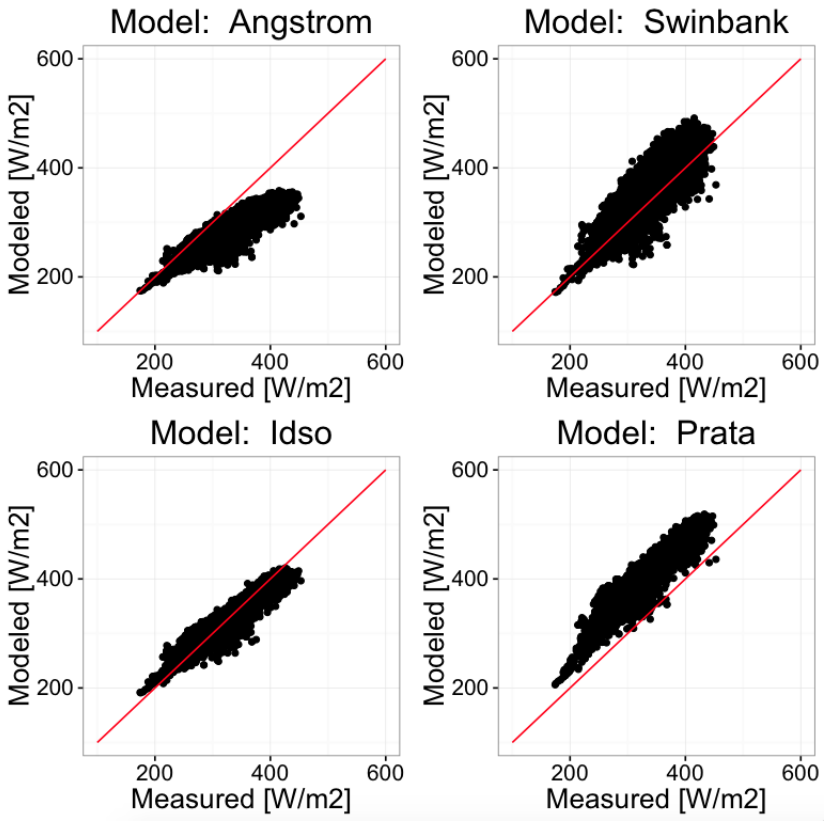

Figure 3: Results of the clear-sky simulation for four literature models using data from Howland Forest (Maine).

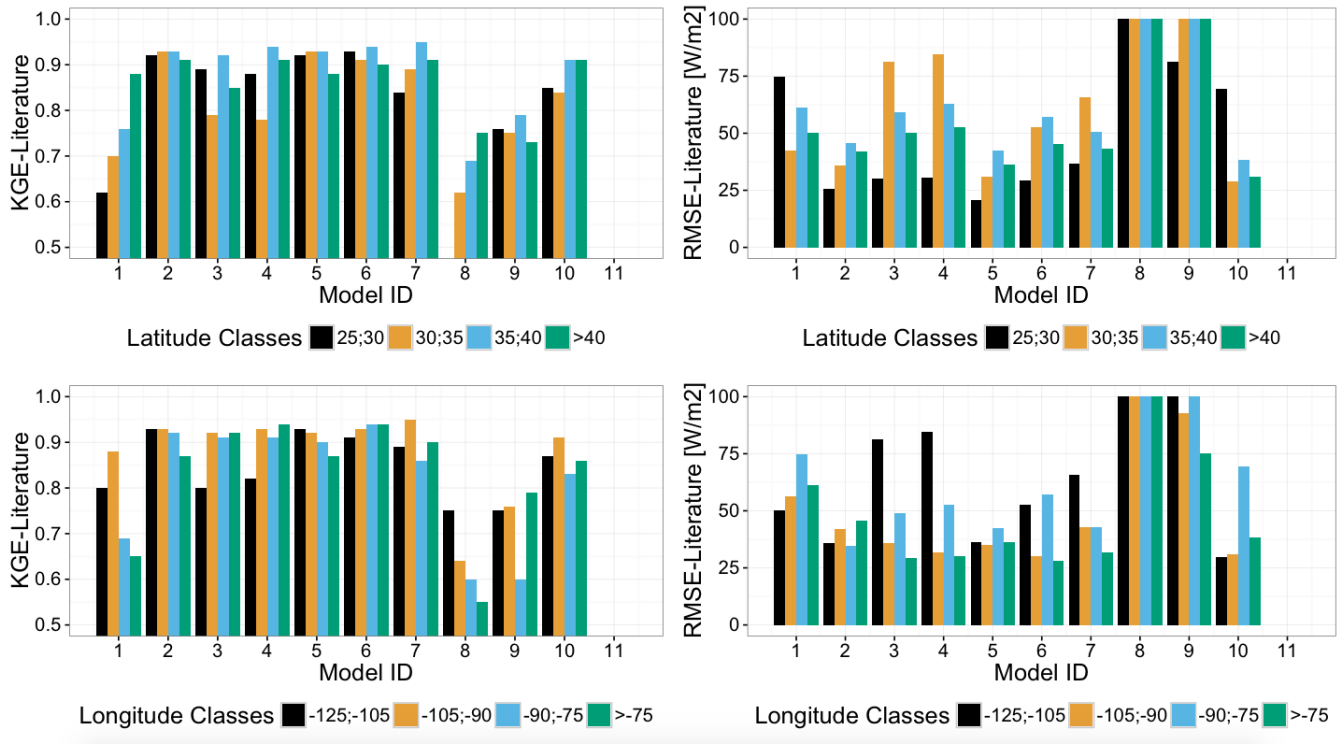

Figure 4: KGE and RMSE values for each clear-sky simulation using literature formulations, grouped by classes of latitude and longitude. The values of the KGE shown are those above 0.5: in this case, model 8 KGE values are not represented as they are between 0.16 and 0.41. The range of RMSE is 0-100 W/m^2.

4.2 $L_{\downarrow}$ models with site-specific parameters

The calibration procedure greatly improves the performances of all ten SMs. Optimized model parameters for each model are reported in the supplementary material. Figure 5 presents the KGE and RMSE values for clear-sky conditions grouped by classes of latitude and longitude. The percentage of KGE improvement ranges from its maximum value of 80% for model 8 (which is not, however, representative of the mean behavior of the SMs) to less than 10% for model 6, with an average improvement of around 35%. Even though variations in model performances with longitude and latitude classes still exist when using optimized model parameters, the magnitude of these variations is reduced with respect to the use of literature formulations. The calibration procedure reduces the RMSE values for all the models to below 50 W/m^2, with the exception of model 8, which now has a maximum of 58 W/m^2.

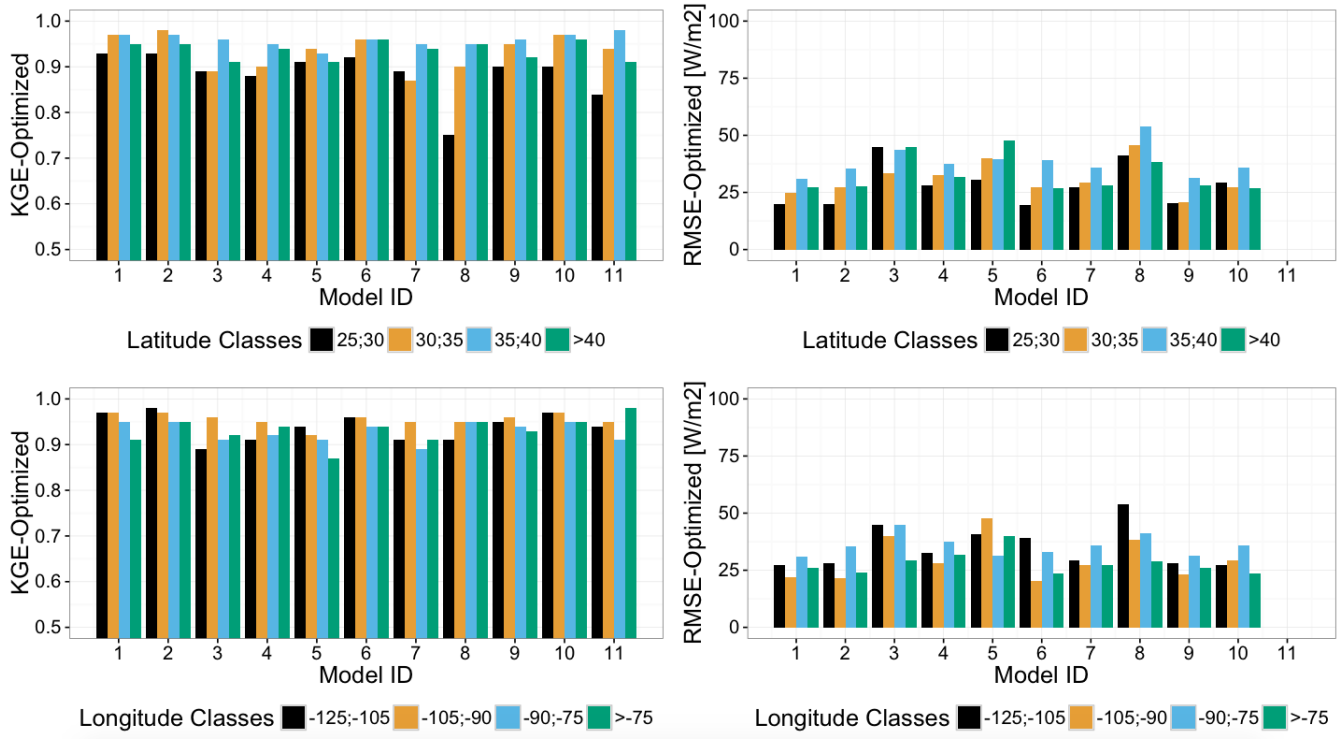

Figure 5: KGE (best is 1) and RMSE (best is 0) values for each optimized formulation in clear-sky conditions, grouped by classes of latitude and longitude. Only values of KGE above 0.5 are shown.

Figure 6 presents KGE and RMSE values for each model under all-sky conditions, grouped by latitude and longitude classes. In general, for all-sky conditions we observe a deterioration of KGE and RMSE values with respect to the clear-sky optimized case, with a decrease in KGE values up to a maximum of 25% for model 10. This may be due to uncertainty incorporated in the formulation of the cloudy-sky correction model (eq. 3): it seems that sometimes the cloud effects are not accounted for appropriately. This, however, is in line with the findings of Carmona et al. (2014).

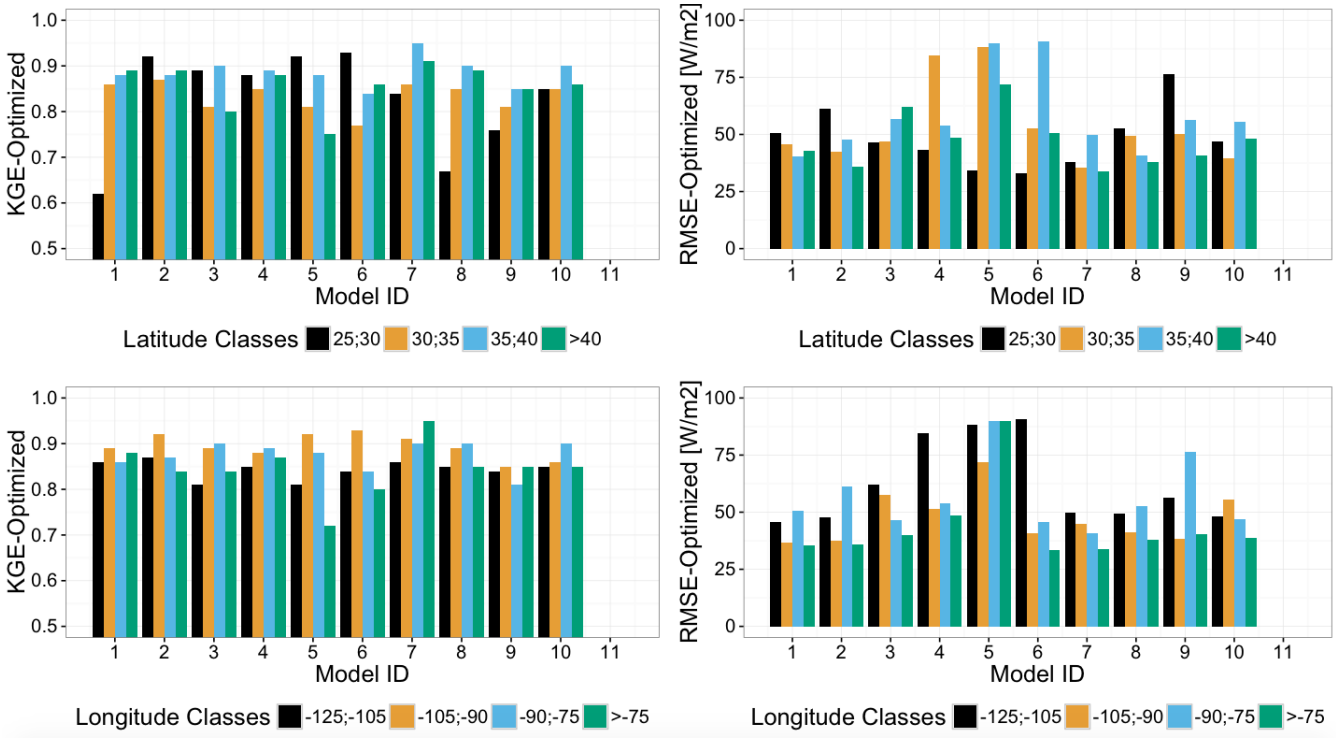

Figure 6: KGE and RMSE values for each model in all-sky conditions, grouped by classes of latitude and longitude. Only values of KGE above 0.5 are shown.

4.3 Sensitivity analysis of $L_{\downarrow}$ models

The results of the models sensitivity analysis are summarized in Figures 7-a and 7-b for models 1 to 5 and models 6 to 10, respectively. Each figure presents three columns, one for each parameter. Considering model 1 and parameter X: the range of X is subdivided into ten equal-sized classes and for each class the corresponding KGE values are presented as a boxplot. A smooth blue line passing through the boxplot medians is added to highlight any possible pattern to parameter sensitivity. A flat line indicates that the model is not sensitive to parameter variation around optimal value. Results suggest that models with one and two parameters are all sensitive to parameter variation, presenting a peak in KGE in correspondence with their optimal values; this is more evident in models with two parameters. Models with three parameters tend to have at least one insensitive parameter, except for model 1, that could reveal a possible overparameterization of the modeling process.

4.4 Regression model for parameters of $L_{\downarrow}$ models

A multivariate linear regression model was estimated to relate the site-specific parameters X, Y and Z to mean annual air temperature, relative humidity, precipitation, and altitude. The script containing the regression model is available, with the supplementary material, at the web page of this paper: *https* : *//github.com/geoframecomponents*.

The performances of the $L_{\downarrow}$ models using parameters assessed by linear regression are evaluated through the leave-one-out cross validation (Efron and Efron, 1982). We use 23 stations as training-sets for equations (6), (7), and (8) and we perform the model verification on the remaining station. The procedure is repeated for each of the 24 stations.

The cross validation results for all $L_{\downarrow}$ models and for all stations are presented in figures (8) and (9), grouped

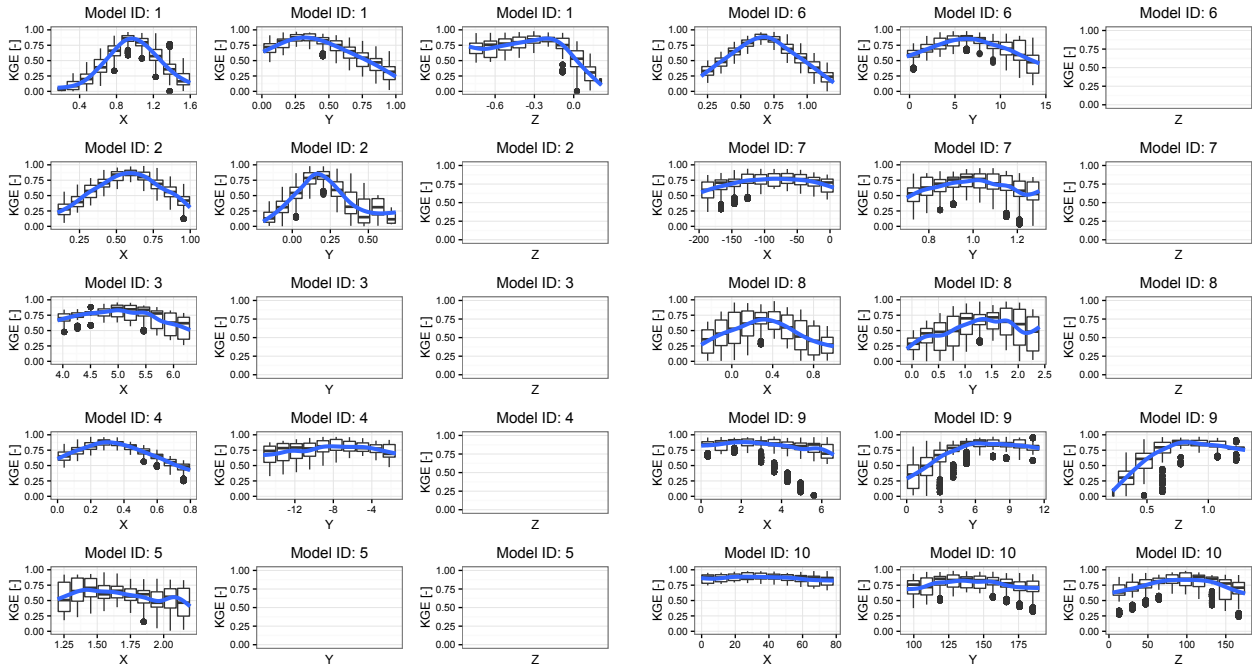

(a) (b)

Figure 7: Results of the model parameters sensitivity analysis. It presents as boxplot the variation of the model performances due to a variation of one of the optimal parameter and assuming constant the others. The procedure is repeated for each model and the blue line represents the smooth line passing through the boxplot medians.

by classes of latitude and longitude, respectively. They report the KGE comparison between the $L_{\downarrow}$ models with their original parameters (in red) and with the regression model parameters (in blue).

In general, the use of parameters estimated with regression model gives a good estimation of $L_{\downarrow}$, with KGE values of up to 0.97. With respect to the classic formulation, model performance with regression parameters improved for all the models, in particular for model 8 in which the KGE improved from a minimum of 0.16 for the classic formulation to a maximum of 0.97.

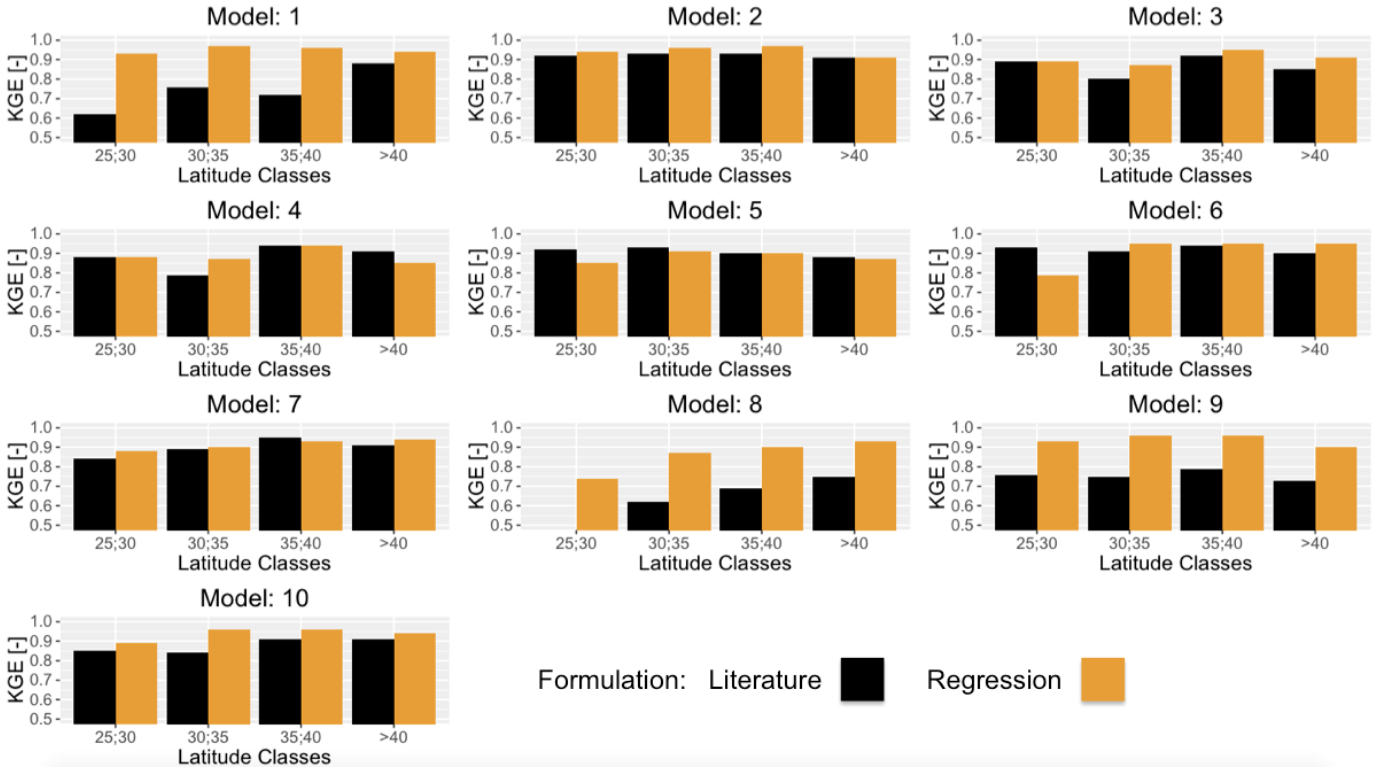

Figure 8: Comparison between model performances obtained with regression and classic parameters: the KGE values shown are those above 0.7 and results are grouped by latitude classes.

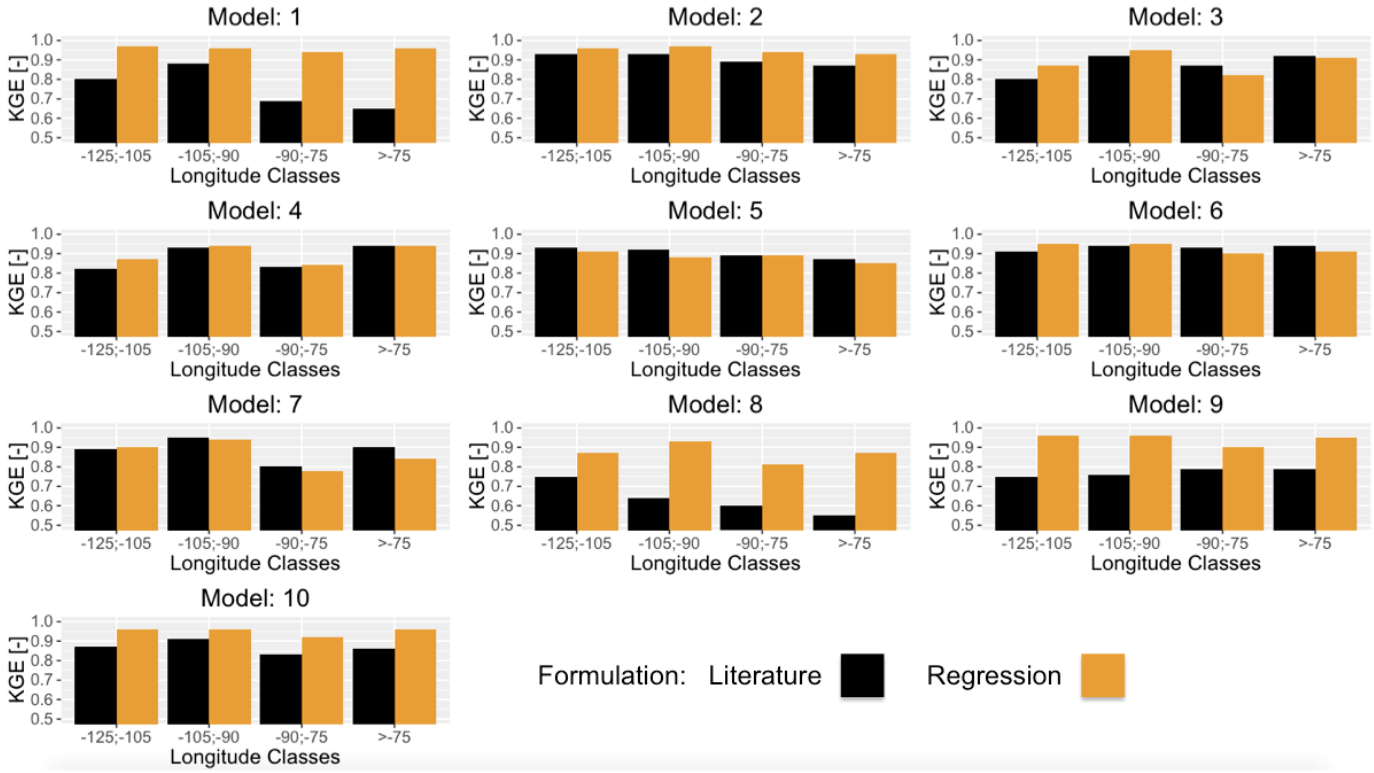

Figure 9: Comparison between model performances obtained with regression and classic parameters: the KGE values shown are those above 0.7 and results are grouped by longitude classes.

4.5 Verification of the $L_{\uparrow}$ model

Figure 10 presents the results of the $L_{\uparrow}$ simulations obtained using the three different temperatures available at experimental sites: soil surface temperature (skin temperature), air temperature, and soil temperature (measured at 4 cm below the surface). The figure shows the performances of the $L_{\uparrow}$ model for the three different temperatures used in terms of KGE, grouping all the stations for the whole simulation period according to season. This highlights the different behaviors of the model for periods where the differences in the three temperatures are larger (winter) or negligible (summer). The values of soil emissivity are assigned according the soil surface type, according to Table 4 (Brutsaert, 2005). Although many studies investigated the influence of snow covered area on longwave energy balance (e.g. Plüss and Ohmura (1997); Sicart et al. (2006)), the SMs do not explicitly take into account of it. As presented in König-Langlo and Augstein (1994), the effect of snow could be implicitly taken into account by tuning the emissivity parameter.

The best fit between measured and simulated $L_{\uparrow}$ is obtained with the surface soil temperature, with an all-season average KGE of 0.80. Unfortunately, the soil surface temperature is not an easily available measurement. In fact, it is available only for 8 sites of the 24 in the study area. Very good results are also obtained using the air temperature, where the all-season average KGE is around 0.76. The results using air temperature present much more variance compared to those obtained with the soil surface temperature. However, air temperature (at 2 m height) is readily available measure, in fact it is available for all 24 sites.

The use soil temperature at 4 cm depth provides the least accurate results for our simulations, with an all-season average KGE of 0.46. In particular, the use of soil temperature at 4 cm depth during the winter is not able to capture the dynamics of $L_{\uparrow}$. It does, however, show a better fit during the other seasons. This could be because during the winter there is a substantial difference between the soil and skin temperatures, as also suggested in Park et al. (2008).

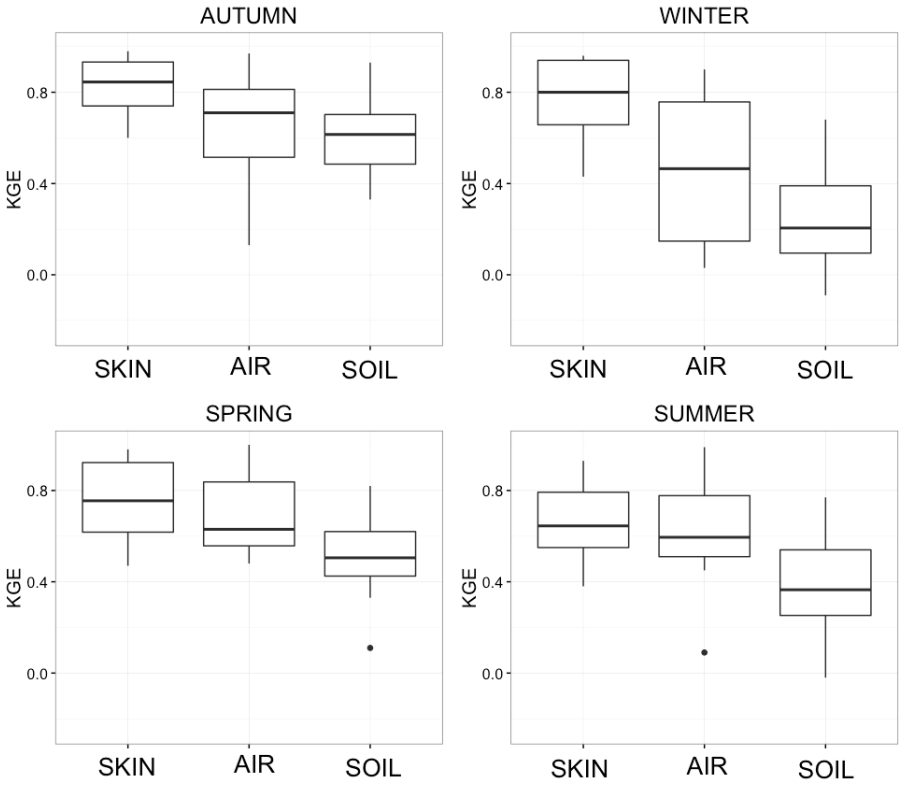

Figure 10: Boxplots of the KGE values obtained by comparing modeled upwelling longwave radiation, computed with different temperatures (soil surface temperature (SKIN), air temperature (AIR), and soil temperature (SOIL)), against measured data. Results are grouped by seasons.

5 Conclusions

This paper presents the LWRB package, a new modeling component integrated into the JGrass-NewAge system to model upwelling and downwelling longwave radiation. It includes ten parameterizations for the computation of $L_{\downarrow}$ longwave radiation and one for $L_{\uparrow}$. The package uses all the features offered by the JGrass-NewAge system, such as algorithms to estimate model parameters and tools for managing and visualizing data in GIS.

The LWRB is tested against measured $L_{\downarrow}$ and $L_{\uparrow}$ data from 24 AmeriFlux test-sites located all over continental USA. The application for $L_{\downarrow}$ longwave radiation involves model parameter calibration, model performance assessment, and parameters sensitivity analysis. Furthermore, we provide a regression model that estimates optimal parameter sets on the basis of local climatic variables, such as mean annual air temperature, relative humidity, and precipitation. The application for $L_{\uparrow}$ longwave radiation includes the evaluation of model performance using three different temperatures.

The main achievements of this work include: i) a broad assessment of the classic $L_{\downarrow}$ longwave radiation parameterizations, which clearly shows that the Idso (1981) and Brunt (1932) models are the more robust and reliable for all the test sites, confirming previous results (Carmona et al., 2014); ii) a site specific assessment of the $L_{\downarrow}$ longwave radiation model parameters for 24 AmeriFlux sites that improved the performances of all the models; iii) the set up of a regression model that provides an estimate of optimal parameter sets on the basis climatic data; iv) an assessment of $L_{\uparrow}$ model performances for different temperatures (skin temperature, air temperature, and soil temperature at 4 cm below surface), which shows that the skin and the air temperature

are better proxy for the $L_{\uparrow}$ longwave radiation. Moreover the Brunt (1932) model is able to provide higher performances with the regression model parameters independently of the latitude and longitude classes. For the Idso (1981) model the formulation with regression parameter provided lower performances respect to the literature formulation for latitude between [25-30].

The integration of the package into JGrass-NewAge will allow users to build complex modeling solutions for various hydrological scopes. In fact, future work will include the link of the LWRB package to the existing components of JGrass-NewAge to investigate $L_{\downarrow}$ and $L_{\uparrow}$ effects on evapotranspiration, snow melting, and glacier evolution. Finally, the methodology proposed in this paper provides the basis for further developments such as the possibility to: i) investigate the effect different all-sky emissivity formulation, ii) verify the usefulness of the regression models for locations outside the USA; iii) analyze in a systematic way the uncertainty due to the quality of meteorological input data on the longwave radiation balance in scarce instrumented areas.

ACKNOWLEDGEMENTS

The authors are grateful to the AmeriFlux research community for providing the high-quality public data sets. In particular, we want to thank the principal investigators of each site: Shirley Kurc Papuga (AZ), Tilden P. Meyers (AZ), Russ Scott (AZ), Tom Kolb (AZ), Sonia Wharton (CA), Dennis D. Baldocchi (CA), Jordan G.Barr (FL), Vic C. Engel (FL), Jose D. Fuentes (FL), Joseph C. Zieman (FL), David Y. Hollinger (ME), Joe McFadden (MN), John M. Baker (MN), Timothy J. Griffis (MN), Lianhong Gu (MO), Kenneth L. Clark (NJ), Dave Billesbach (OK), James A. Bradford (OK), Margaret S. Torn (OK), James L. Heilman (TX), Ken Bible (WA), Sonia Wharton (WA). The authors thank the CLIMAWARE Project, of the University of Trento (Italy), and the GLOBAQUA Project, which have supported their research.

Replicable Research

Researchers interested in replicating or extending our results are invited to download our codes at:

https : *//github.com/geoframecomponents*.

Instructions for using the code can be found at:

http : *//geoframe.blogspot.co.uk*/2016/04/*lwrb* − *component* − *latest* − *documentation.html*.

Regression of parameters were performed in R and are available at

https : *//github.com/GEOframeOMSProjects/OMS_Project_LWRB/blob/master/docs/Regression.R*

References

L Alados-Arboledas, J Vida, and FJ Olmo. The estimation of thermal atmospheric radiation under cloudy conditions. *International journal of climatology*, 15(1):107–116, 1995.

Anders Knutsson Ångström. *A study of the radiation of the atmosphere: based upon observations of the nocturnal radiation during expeditions to Algeria and to California*, volume 65. Smithsonian Institution, 1915.

John A Augustine, John J DeLuisi, and Charles N Long. Surfrad-a national surface radiation budget network for atmospheric research. *Bulletin of the American Meteorological Society*, 81(10):2341–2357, 2000.

John A Augustine, Gary B Hodges, Christopher R Cornwall, Joseph J Michalsky, and Carlos I Medina. An update on surfrad-the gcos surface radiation budget network for the continental united states. *Journal of Atmospheric and Oceanic Technology*, 22(10):1460–1472, 2005.

Dennis Baldocchi, Eva Falge, Lianhong Gu, Richard Olson, David Hollinger, Steve Running, Peter Anthoni, Ch Bernhofer, Kenneth Davis, Robert Evans, et al. Fluxnet: A new tool to study the temporal and spatial variability of ecosystem-scale carbon dioxide, water vapor, and energy flux densities. *Bulletin of the American Meteorological Society*, 82(11):2415–2434, 2001.

Jordan G Barr, Vic Engel, Thomas J Smith, and José D Fuentes. Hurricane disturbance and recovery of energy balance, co 2 fluxes and canopy structure in a mangrove forest of the florida everglades. *Agricultural and Forest Meteorology*, 153:54–66, 2012.

HM Bolz. Die abhängigkeit der infraroten gegenstrahlung von der bewölkung. *Z Meteorol*, 3:201–203, 1949.

David Brunt. Notes on radiation in the atmosphere. i. *Quarterly Journal of the Royal Meteorological Society*, 58(247):389–420, 1932.

Wilfried Brutsaert. On a derivable formula for long-wave radiation from clear skies. *Water Resources Research*, 11(5):742–744, 1975.

Wilfried Brutsaert. *Hydrology: an introduction*, volume 61. Wiley Online Library, 2005.

Gaylon S Campbell. *Soil physics with BASIC: transport models for soil-plant systems*, volume 14. Elsevier, 1985.

Facundo Carmona, Raúl Rivas, and Vicente Caselles. Estimation of daytime downward longwave radiation under clear and cloudy skies conditions over a sub-humid region. *Theoretical and applied climatology*, 115 (1-2):281–295, 2014.

John M Chambers, TJ Hastie, et al. Linear models, 1992.

Javier Gonzalez Corripio. *Modelling the energy balance of high altitude glacierised basins in the Central Andes*. PhD thesis, University of Edinburgh, 2002.

Todd M Crawford and Claude E Duchon. An improved parameterization for estimating effective atmospheric emissivity for use in calculating daytime downwelling longwave radiation. *Journal of Applied Meteorology*, 38 (4):474–480, 1999.

O David, JC Ascough, W Lloyd, TR Green, KW Rojas, GH Leavesley, and LR Ahuja. A software engineering perspective on environmental modeling framework design: The object modeling system. *Environmental Modelling & Software*, 39:201–213, 2013.

QY Duan, Vijai K Gupta, and Soroosh Sorooshian. Shuffled complex evolution approach for effective and efficient global minimization. *Journal of optimization theory and applications*, 76(3):501–521, 1993.

Bradley Efron and B Efron. *The jackknife, the bootstrap and other resampling plans*, volume 38. SIAM, 1982.

GN Flerchinger. The simultaneous heat and water (shaw) model: Technical documentation, northwest watershed research center, usda agricultural research service, boise. Technical report, Idaho, Technical Report NWRC 2000-09, 37 pp, 2000.

GN Flerchinger, Wei Xaio, Danny Marks, TJ Sauer, and Qiang Yu. Comparison of algorithms for incoming atmospheric long-wave radiation. *Water resources research*, 45(3), 2009.

G Formetta, R Rigon, JL Chávez, and O David. Modeling shortwave solar radiation using the jgrass-newage system. *Geoscientific Model Development*, 6(4):915–928, 2013.

G Formetta, A Antonello, S Franceschi, O David, and R Rigon. Hydrological modelling with components: A gis-based open-source framework. *Environmental Modelling & Software*, 55:190–200, 2014a.

G Formetta, O David, and R Rigon. Testing site-specific parameterizations of longwave radiation integrated in a gis-based hydrological model. *International Environmental Modelling and Software Society (iEMSs) 7th Intl. Congress on Env. Modelling and Software, San Diego, CA, USA, Daniel P. Ames, Nigel W.T. Quinn and Andrea E. Rizzoli (Eds.)*, 2014b.

Hoshin V Gupta, Harald Kling, Koray K Yilmaz, and Guillermo F Martinez. Decomposition of the mean squared error and nse performance criteria: Implications for improving hydrological modelling. *Journal of Hydrology*, 377(1):80–91, 2009.

JL Hatfield, R Jl Reginato, and SB Idso. Comparison of long-wave radiation calculation methods over the united states. *Water Resources Research*, 19(1):285–288, 1983.

Lauren E Hay, George H Leavesley, Martyn P Clark, Steve L Markstrom, Roland J Viger, and Makiko Umemoto. Step wise, multiple objective calibration of a hydrologic model for a snowmelt dominated basin1, 2006.

Sherwood B Idso. A set of equations for full spectrum and 8-to 14-μm and 10.5-to 12.5-μm thermal radiation from cloudless skies. *Water resources research*, 17(2):295–304, 1981.

Sherwood B Idso and Ray D Jackson. Thermal radiation from the atmosphere. *Journal of Geophysical Research*, 74(23):5397–5403, 1969.

MOSES G Iziomon, HELMUT Mayer, and ANDREAS Matzarakis. Downward atmospheric longwave irradiance under clear and cloudy skies: Measurement and parameterization. *Journal of Atmospheric and Solar-Terrestrial Physics*, 65(10):1107–1116, 2003a.

MOSES G Iziomon, HELMUT Mayer, and ANDREAS Matzarakis. Downward atmospheric longwave irradiance under clear and cloudy skies: Measurement and parameterization. *Journal of Atmospheric and Solar-Terrestrial Physics*, 65(10):1107–1116, 2003b.

JD Jacobs. Radiation climate of broughton island. *Energy budget studies in relation to fast-ice breakup processes in Davis Strait*, 26:105–120, 1978.

I Juszak and F Pellicciotti. A comparison of parameterizations of incoming longwave radiation over melting glaciers: model robustness and seasonal variability. *Journal of Geophysical Research: Atmospheres*, 118(8): 3066–3084, 2013.

I Keding. *Klimatologische Untersuchung ueber die atmosphaerische Gegenstrahlung und Vergleich vom Berechnungsverfahren anhand langjaehriger Messungen im Oberrheintal*. Offenbach am Main: Selbstverlag des Deutschen Wetterdienstes, 1989.

FM Kelliher, DJ Ross, BE Law, DD Baldocchi, and NJ Rodda. Limitations to carbon mineralization in litter and mineral soil of young and old ponderosa pine forests. *Forest Ecology and Management*, 191(1):201–213, 2004.

Jeffrey R Key and Axel J Schweiger. Tools for atmospheric radiative transfer: Streamer and fluxnet. *Computers & Geosciences*, 24(5):443–451, 1998.

Francis X Kneizys, EP Shettle, LW Abreu, JH Chetwynd, and GP Anderson. Users guide to lowtran 7. Technical report, DTIC Document, 1988.

Gert König-Langlo and Ernst Augstein. Parameterization of the downward long-wave radiation at the earth's surface in polar regions. *Meteorologische zeitschrift, NF 3, Jg. 1994, H. 6*, pages 343–347, 1994.

Thomas Konzelmann, Roderik SW van de Wal, Wouter Greuell, Richard Bintanja, Edwin AC Henneken, and Ayako Abe-Ouchi. Parameterization of global and longwave incoming radiation for the greenland ice sheet. *Global and Planetary change*, 9(1):143–164, 1994.

Egbert Giles Leigh Jr. *Tropical Forest Ecology: A View from Barro Colorado Island: A View from Barro Colorado Island*. Oxford University Press, 1999.

Shelley MacDonell, Lindsey Nicholson, and Christophe Kinnard. Parameterisation of incoming longwave radiation over glacier surfaces in the semiarid andes of chile. *Theoretical and applied climatology*, 111(3-4):513–528, 2013.

Gary A Maykut and Phil E Church. Radiation climate of barrow alaska, 1962-66. *Journal of Applied Meteorology*, 12(4):620–628, 1973.

John Lennox Monteith and MH Unsworth. *Principles of Environmental Physics*. Butterworth-Heinemann, 1990.

Sami Niemelä, Petri Räisänen, and Hannu Savijärvi. Comparison of surface radiative flux parameterizations: Part i: Longwave radiation. *Atmospheric Research*, 58(1):1–18, 2001.

Gi-Hyeon Park, Xiaogang Gao, and Soroosh Sorooshian. Estimation of surface longwave radiation components from ground-based historical net radiation and weather data. *Journal of Geophysical Research: Atmospheres (1984–2012)*, 113(D4), 2008.

Christian Plüss and Atsumu Ohmura. Longwave radiation on snow-covered mountainous surfaces. *Journal of Applied Meteorology*, 36(6):818–824, 1997.

AJ Prata. A new long-wave formula for estimating downward clear-sky radiation at the surface. *Quarterly Journal of the Royal Meteorological Society*, 122(533):1127–1151, 1996.

E Rotenberg, Y Mamane, and JH Joseph. Long wave radiation regime in vegetation-parameterisations for climate research. *Environmental modelling & software*, 13(3):361–371, 1998.

Edgar Schmucki, Christoph Marty, Charles Fierz, and Michael Lehning. Evaluation of modelled snow depth and snow water equivalent at three contrasting sites in switzerland using snowpack simulations driven by different meteorological data input. *Cold Regions Science and Technology*, 99:27–37, 2014.

Jean-Emmanuel Sicart, JW Pomeroy, RLH Essery, and D Bewley. Incoming longwave radiation to melting snow: observations, sensitivity and estimation in northern environments. *Hydrological processes*, 20(17):3697–3708, 2006.

M Sugita and W Brutsaert. Comparison of land surface temperatures derived from satellite observations with ground truth during fife. *International Journal of Remote Sensing*, 14(9):1659–1676, 1993a.

Michiaki Sugita and Wilfried Brutsaert. Cloud effect in the estimation of instantaneous downward longwave radiation. *Water Resources Research*, 29(3):599–605, 1993b.

Michael H Unsworth and JL Monteith. Long-wave radiation at the ground i. angular distribution of incoming radiation. *Quarterly Journal of the Royal Meteorological Society*, 101(427):13–24, 1975.

GN Wilkinson and CE Rogers. Symbolic description of factorial models for analysis of variance. *Applied Statistics*, pages 392–399, 1973.

Jingfeng Xiao, Qianlai Zhuang, Beverly E Law, Jiquan Chen, Dennis D Baldocchi, David R Cook, Ram Oren, Andrew D Richardson, Sonia Wharton, Siyan Ma, et al. A continuous measure of gross primary production for the conterminous united states derived from modis and ameriflux data. *Remote sensing of environment*, 114(3):576–591, 2010.